THE JOURNAL OF PHYSICAL CHEMISTRY C

Article

pubs.acs.org/JPCC

Evolution Pathway of CIGSe Nanocrystals for Solar Cell Applications

Mahshid Ahmadi,[†] Stevin Snellius Pramana,[‡] Lifei Xi,[†] Chris Boothroyd,[⊥] Yeng Ming Lam,*[,†,§,∥] and Subodh Mhaisalkar[†,§]

[†]School of Materials Science and Engineering, and [‡]Facility for Analysis, Characterization, Testing and Simulation, Nanyang Technological University, 50 Nanyang Avenue, 639798, Singapore

[§]Energy Research Institute @ NTU, Nanyang Technological University, 50 Nanyang Drive, 637553, Singapore

[∥]Institut für Werkstoffe der Elektrotechnik II, RWTH Aachen, Sommerfeldstraße 24, D-52074 Aachen, Germany

[⊥]Ernst Ruska-Centrum und Peter Grünberg Institut, Forschungszentrum Jülich, D-52425 Jülich, Germany

Supporting Information

ABSTRACT: $CuIn_xGa_{1-x}Se_2$ nanocrystals synthesized via the hot injection route have been used to make thin film solar cells with high power conversion efficiency. Thus, $CuIn_xGa_{1-x}Se_2$ nanocrystals have the potential to provide a low cost and high efficiency solution to harvest solar energy. Stoichiometry control of these nanocrystals offers the possibility of tuning the band gap of this material. It is important to understand how the composition of quaternary $CuIn_xGa_{1-x}Se_2$ nanocrystals evolves to control the stoichiometry of this compound. We report a systematic study of the growth and evolution pathways of quaternary $CuIn_{0.5}Ga_{0.5}Se_2$ nanocrystals in a hot coordination solvent. The reaction starts by the formation of a mixture of binary and ternary nanocrystals, which transforms subsequently to $CuIn_{0.5}Ga_{0.5}Se_2$ nanocrystals. These binary and ternary compounds dissolve in the course of the reaction, so as to provide the molecular precursor for monophasic $CuIn_{0.5}Ga_{0.5}Se_2$ nanocrystals to form. Here, we study the growth sequence of these spherical, monophasic $CuIn_{0.5}Ga_{0.5}Se_2$ nanocrystals as a function of time. Control experiments indicated that the phase changes of $CuIn_{0.5}Ga_{0.5}Se_2$ nanocrystals are temperature- and time-dependent. The change in the stoichiometry of $CuIn_{0.5}Ga_{0.5}Se_2$ during growth was estimated using Vegard's law.

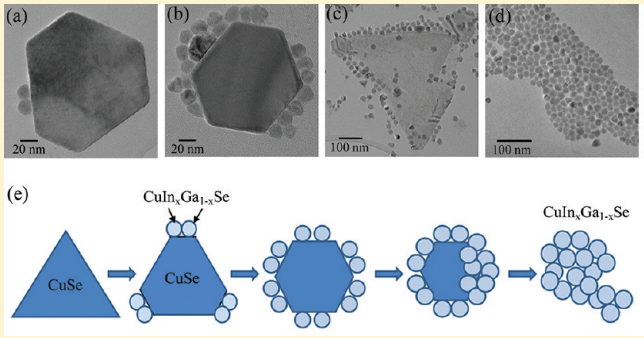

1. INTRODUCTION

In the last two decades, inorganic semiconductor nanocrystals have drawn much attention due to their potential applications in different industries.[1,2] Many researchers, both in academia and in industry, have focused their effort on synthesizing high-quality and size tunable nanocrystals using chemical methods.[3] A variety of wet chemical synthesis routes including solvothermal, hot injection, and other colloidal methods have been developed,[3−13] focusing mainly on controlling the size and size distribution of the nanoparticles and reducing the extensive purification steps. Hot injection has been shown to give rise to well-controlled size, morphology, and stoichiometry.

Ternary and quaternary chalcogenides have been widely used in areas such as photovoltaic cells,[14−17] optoelectronic devices,[18,19] light-emitting diodes,[20,21] and biomedical devices[22] due to their outstanding electrical and optical properties. One of the most widely studied chalcogenides is quaternary $CuIn_xGa_{1-x}Se_2$. They are commonly used as light absorbers to harvest solar energy because of their high absorption coefficient ($\alpha \approx 5 \times 10^5$ cm^{-1}), tunable energy band gap (1.07−1.7 eV),[23] which is complementary to the solar spectrum (1.1−1.5 eV), and low toxicity.[24−26] Research has shown that solution-phase processes based on the $Cu(In_xGa_{1-x})(S_ySe_{1-y})_2$ family of nanocrystal inks synthesized using the hot injection method to make low cost solar cells have yielded efficiencies close to 5%.[27,28]

In the past decade, great progress has been made in the controlled synthesis of colloidal monodisperse binary chalcogenides and other functional compounds through the hot injection approach. In contrast to the improvement in the synthesis of binary chalcogenides,[3,29−31] synthesis of ternary or quaternary $CuIn_xGa_{1-x}Se_2$ nanocrystals is still challenging due to the difficulty in controlling the stoichiometry of the nanocrystals. This is because phase separation can easily occur between the various possible solid-solution components, caused mainly by the lattice mismatch between each constituent and also by the differences in the reactivity of precursors.[32] Some efforts to synthesize $CuIn_xGa_{1-x}S_2$ (CIGS) or $CuIn_xGa_{1-x}Se_2$ (CIGSe) nanoparticles using coordinating solvent (e.g., OLA and TOPO) or noncoordinating solvent (ODE) by the hot injection method have been reported.[27,28,33−36] In general, quaternary $CuIn_xGa_{1-x}Se_2$ nanocrystals as compared to the

Received: January 6, 2012
Revised: March 9, 2012
Published: March 9, 2012

equivalent bulk materials have poor uniformity in both composition and phase. This is not unexpected because the system has a very complicated phase diagram and the nanocrystals formed can further increase the phase complexity.[37]

It is important to have a precise control over the chemical composition, crystal structure, size, and shape of inorganic nanocrystals to be able to tune their optical and electrical properties to improve the performance of solar cells.[4,38] Another important characteristic of quaternary nanocrystals for their application in solar cells is the purity of the phase so as to generate a single band gap within each junction. Although there were some reports that mentioned the formation of a single phase of solid solution $CuIn_{0.5}Ga_{0.5}Se_2$, their XRD peaks showed split reflections, which indicate a mixture of different $CuIn_xGa_{1-x}Se_2$ phases.[35,39,40] As a result, properties such as the band gap may not be optimal for good device performance. Thus, in this work the synthesis of monodisperse, single-crystalline, and single-phase nanoparticles of CIGSe is studied, which is crucial in the control of its properties and hence its application in photovoltaics. These ternary and quarternary compounds are frequently synthesized using OLA. In the present work, hexadecylamine (HDA) was shown for the first time to be able to control the growth of CIGSe nanocrystals very well. Both HDA and OLA are very similar ligands/solvents. OLA ($C_{18}H_{37}N$) and HDA ($C_{16}H_{35}N$) are from the same family of primary amines, and synthesis pathways of CIGSe nanocrystals using HDA or OLA should not deviate much as the functionality of both ligands is very similar. The synthesis of nanocrystals using HDA and OLA gives similar morphology and sizes, but HDA has the advantage of having shorter chain, which usually gives a better degree of monodispersity in the synthesis of nanocrystals.[41−43]

Understanding the growth and formation pathway of ternary and quaternary $CuIn_xGa_{1-x}Se_2$ is important to reach a stoichiometric compound and improve the growth of nanocrystals. A few successful attempts have been made to control the evolution of ternary CIS and CISe nanocrystals.[44,45] However, the nucleation and growth mechanism of quaternary CIGSe nanoparticles is still unclear, which makes determination of the processes and transformation states of these nanoparticles difficult. Therefore, investigation of the pathways for pure quaternary CIGSe during hot injection synthesis is required to further comprehend the phase, composition, size, and morphology development. This Article presents a growth sequence for quaternary CIGSe during hot injection synthesis. Although the synthesis reported is a one-pot reaction, the formation of $CuIn_{0.5}Ga_{0.5}Se_2$ nanocrystals involves several steps.

2. EXPERIMENTAL DETAILS

2.1. $CuIn_{0.5}Ga_{0.5}Se_2$ Nanocrystal Synthesis. In this study, the growth of monodisperse, pure $CuIn_{0.5}Ga_{0.5}Se_2$ nanocrystals using hot injection synthesis is systematically studied. The nanocrystals were synthesized using a modified hot injection process where hexadecylamine (HDA) is the capping reagent and some simple precursors, for example, metal acetylacetonate, chloride, and elemental selenium, are used. The processes were carried out in an oxygen-free environment. The products obtained are readily dispersed in organic solvents such as toluene and chloroform.

A typical procedure for $CuIn_{0.5}Ga_{0.5}Se_2$ synthesis is as follows: 0.2 mmol of CuCl (Sigma-Aldrich, 99.995%), 0.1 mmol of $InCl_3$ (Sigma-Aldrich, 99.999%), and 0.1 mmol of gallium(III) acetylacetonate ($Ga(acac)_3$, Sigma-Aldrich, anhydrous ≥99.999%) were mixed with 6.5 g of *n*-hexadecylamine (HDA, Sigma-Aldrich, 95%) in a three-neck flask at room temperature. The reaction was heated to 80 °C and degassed for 1 h. The complete dissolution of cation precursors at 130 °C was confirmed by a color change in the solution from blue to yellow. A suspension of 0.4 mmol of selenium powder (Se, Kanto Chemical Co. Inc., 99.0%) in 4 g of HDA was heated to 50 °C and injected into the reaction flask at 130 °C under constant stirring and nitrogen flow. This resulted in an immediate color change in the solution to black followed by a temperature drop to 120 °C. Small aliquots were extracted at different temperature and time intervals (different growth conditions) between 10 and 120 min while the reaction was progressing to 230 °C (Figure S1). The reaction was halted by freezing in an ice bath for further investigation of the $CuIn_{0.5}Ga_{0.5}Se_2$ formation progress, and the particles were precipitated and washed with toluene and methanol to remove any residual capping agent. The purified precipitate was subsequently redissolved in toluene.

2.2. Materials Characterization. For optical characterization, the nanocrystals were dispersed in toluene. The ultraviolet−visible/near-infrared (UV−vis/NIR) absorption spectrum of the nanoparticles was obtained using a UV−vis/NIR PerkinElmer Lambda 900 spectrophotometer at room temperature and under ambient conditions with wavelengths ranging from 300 to 1300 nm (step size of 0.5 nm). The size and morphology of the nanocrystals was characterized using transmission electron microscopy (TEM), selected area electron diffraction (SAED), and convergent beam electron diffraction (CBED). Samples for TEM were prepared by dropping nanocrystals dispersed in toluene onto lacey carbon-coated copper grids. TEM studies were carried out using a JEOL 2100F field-emission microscope at an acceleration voltage of 200 kV. The composition of the as-prepared $CuIn_{0.5}Ga_{0.5}Se_2$ nanoparticles was semiquantitatively determined using energy dispersive X-ray spectroscopy (EDAX) in the TEM. The phase and crystallographic structure of the nanocrystals were characterized using grazing incidence X-ray diffraction (GIXRD) patterns, which were recorded using a Bruker D8 Advance with a fixed θ of 0.5°, scanning rate of 0.2° min^{-1}, step size of 0.02°, and 2θ range from 10 to 80°, using CuK_α radiation (λ_{ave} = 1.54 Å) operating at 40 kV and 40 mA. The starting Rietveld refinement model used CuSe,[46] Se,[47] $CuInSe_2$,[48] $CuGaSe_2$,[49] and $CuIn_{0.52}Ga_{0.48}Se_2$.[50] The fundamental parameters peak-shape profile was used; a five-coefficient Chebychev polynomial and $1/x$ background, zero error, scale factors, unit cell parameters, and crystal size were sequentially refined using the TOPAS V4 program. The weight percentage of each phase was calculated on the basis of quantitative phase analysis using the Rietveld method:[51]

$$W_\alpha = \frac{S_\alpha (ZMV)_\alpha}{\sum_i (S_i (ZMV)_i)} \quad (1)$$

where W_α is the weight fraction of phase α, S is the Rietveld scale factor, Z is the number of formula units in unit cell, M is the molecular mass of formula unit, and V is the unit cell volume.

3. RESULTS AND DISCUSSION

At 230 °C (120 min), single-phase tetragonal $CuIn_{0.5}Ga_{0.5}Se_2$ nanocrystals with a relatively narrow size distribution and uniform shape were obtained (Figure 1). To understand the

dx.doi.org/10.1021/jp300187r | J. Phys. Chem. C 2012, 116, 8202−8209

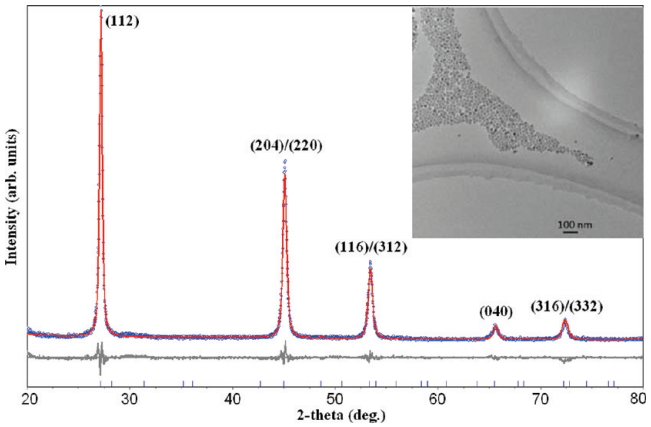

Figure 1. X-ray diffraction pattern of phase pure tetragonal $CuIn_{0.5}Ga_{0.5}Se_2$ nanocrystals synthesized for 120 min at 230 °C. The difference between the calculated (red) and experimental (blue) intensities is shown in gray with the Bragg markers shown at the bottom. The low magnification TEM image of the $CuIn_{0.5}Ga_{0.5}Se_2$ nanocrystals synthesized at 230 °C exhibiting monodispersed size and shape is shown in the inset.

formation of $CuIn_{0.5}Ga_{0.5}Se_2$ nanocrystals and their phase evolution, controlled extractions were carried out at specific reaction intervals. Because of the complexity of the reaction, intermediate pathways for formation of the products need to be accounted for. As was previously studied using thermogravimetric analysis,[52] these precursors have different thermal decomposition temperatures. In general, the precursor reaction with HDA to form the precursor complexes occurs at a lower temperature than the decomposition temperature[53] so it would be difficult to relate the decomposition temperature directly with the activity of the complex. Nevertheless, in this reaction, a narrow size distribution and a uniform shape is obtained using HDA, which acts as both the solvent in the reaction and also the stabilizer to control the activity of the monomers.[41−43] In other words, it is the activation agent, and it may reduce the differences in the reactivity of the precursors and hence assist the formation of homogeneous CIGSe nanoparticles.

3.1. Crystal Chemistry of Cu−In−Ga−Se Phase Evolution. At the start of the reaction (10 min after injection of Se-HDA), a mixture of different phases (CuSe, Se, and $CuGaSe_2$) was formed. The phase distribution can be seen in Table S1. The variation in the XRD background in Figure 2 may arise from the presence of an amorphous phase in the sample. From TEM (EDX), amorphous In_2Se_3 was found (Figure S2a). Se nanorods (12 ± 1 wt %) crystallized upon injection of Se into the reaction, leading to partial consumption of Se in the HDA (Figure S2b). The major phase was found to be binary CuSe nanocrystals (57 ± 1 wt %) (Figure 2a). This is found to be the intermediate step in the growth of $CuIn_{0.5}Ga_{0.5}Se_2$ nanocrystals. Lattice fringe spacings are obtained from the high-resolution transmission electron microscopy (HRTEM) images and SAED patterns (Figure S3a). The spacings are found to be d_1 = 3.32 Å, d_2 = 3.33 Å that correspond to the (010) and (100) lattice planes of hexagonal $P6_3/mmc$ CuSe, respectively. The Cu:Se ratio was close to 1:1 as determined by semi-quantitative EDX analysis, which is consistent with one of the phases determined using XRD. In addition, the XRD pattern also revealed the presence of crystalline ternary $CuGaSe_2$ nanocrystals (31 ± 1 wt %) and was further confirmed by HRTEM and CBED. The interplanar spacings determined from HRTEM/CBED are d_1 = 1.93 Å,

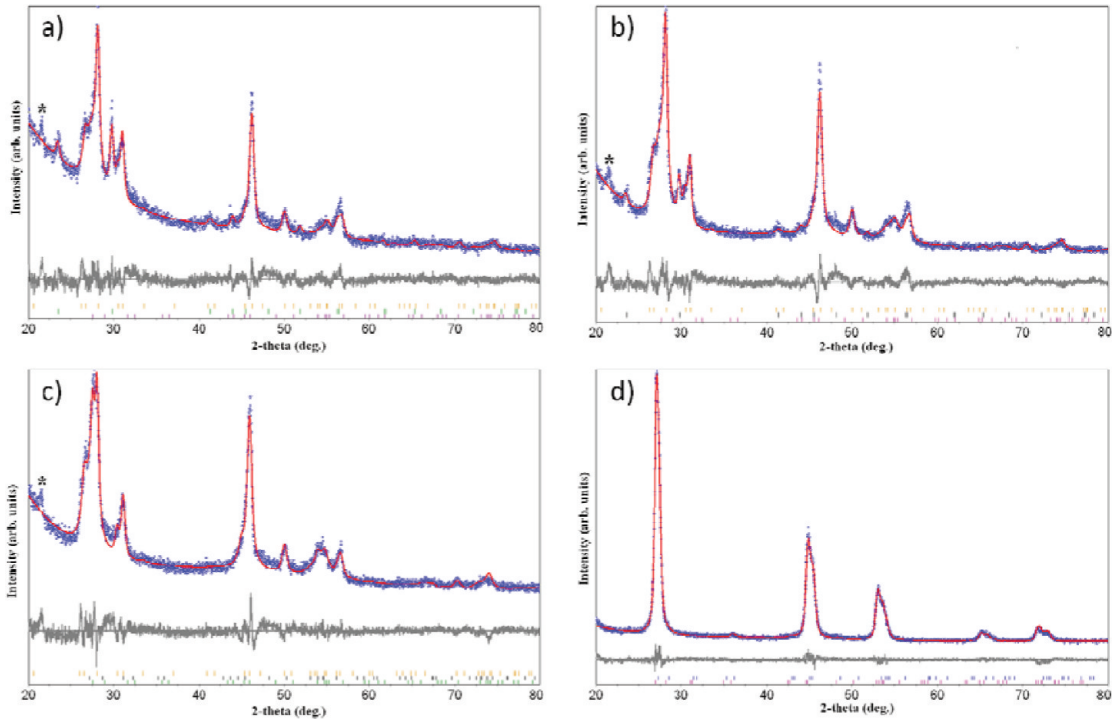

Figure 2. X-ray diffraction patterns and Rietveld refinement of nanocrystals grown for (a) 10 min at 130 °C, (b) 20 min at 160 °C, (c) 40 min at 200 °C, and (d) 60 min at 230 °C. Vertical lines show the positions of Bragg peaks, and the Bragg markers from top to bottom are: (a) and (b) CuSe, Se, and $CuGaSe_2$; (c) CuSe, CIGSe1, and CIGSe2; (d) CIGSe1 and CIGSe2. The gray line is the difference between the calculated and experimental intensities. The blue dots correspond to experimental, and the red line corresponds to calculated intensities. The peak marked "*" corresponds to a diffraction peak from hexadecylamine.

dx.doi.org/10.1021/jp300187r | J. Phys. Chem. C 2012, 116, 8202−8209

d_2 = 1.93 Å, and d_3 = 1.94 Å corresponding to the $(20\bar{4})$, $(02\bar{4})$, and $(\bar{2}20)$ crystal planes (Figure 3a and b).

As the reaction extended to 20 min (160 °C), a mixture of the phases CuSe, Se, and $CuGaSe_2$ could still be observed (Figure 2b). However, the amount of unreacted Se was reduced to 5 ± 1 wt % and was accompanied by an increase in the $CuGaSe_2$ nanocrystal content to (41 ± 1 wt %) (Table S1).

After 40 min, all of the Se had reacted as the temperature reached close to the melting point of Se (217 °C). XRD (Figure 2c) and TEM (Figures 3e,f and S3b) revealed that main phases, 48 ± 1 wt % CuSe and 52 ± 1 wt % $CuIn_xGa_{1-x}Se_2$, coexisted. Rietveld refinement indicated that two quaternary $CuIn_xGa_{1-x}Se_2$ phases with different In/Ga stoichiometries and crystallite sizes were formed (Tables S1 and S2). One of the phases developed from $CuGaSe_2$ nanocrystals has x very close to 0.11 and grew from 8 to 16 nm in 20 min, and, at the same time, a second quaternary $CuIn_xGa_{1-x}Se_2$ started to crystallize (4 nm). The size of each crystallite was calculated using the volume weighted mean crystallite size in a modified Scherrer equation.[54,55]

All of the binary CuSe was consumed to form $CuIn_xGa_{1-x}Se_2$ nanocrystals after 60 min. At this stage, the XRD background indicated that no amorphous In_2Se_3 was left in the sample (Figure 2d). Closer inspection of the $CuIn_xGa_{1-x}Se_2$ XRD peaks clearly shows that biphasic $CuIn_xGa_{1-x}Se_2$ crystallized with different stoichiometry and an average crystal size of 13 ± 1 nm (2θ = 27.1°, 45.1°, and 53.4°) (Figure 2d, Tables S1 and S2). Finally, by extending the reaction time at 230 °C for another 60 min, $CuIn_xGa_{1-x}Se_2$ evolved into single-phase $CuIn_{0.5}Ga_{0.5}Se_2$ nanocrystals with a narrow size distribution (average crystallite size of 20 nm) and a nearly spherical shape. The size of the nanoparticles determined by the Rietveld refinement (Table S1) is consistent with TEM observations (Figure 3i and j).

3.2. $CuIn_xGa_{1-x}Se_2$ Phase Formation and Reaction Mechanism. As discussed earlier, metal−HDA complexes were formed when CuCl, $InCl_3$, and $Ga(acac)_3$ in HDA were heated to 130 °C. Once Se is injected at 130 °C, nucleation of the various phases will start to occur as the metal−HDA complex decomposes and reacts. In stage 1, amorphous In_2Se_3, CuSe, and $CuGaSe_2$ nanocrystals and unreacted Se nanorods were formed. The reason for the initial formation of CuSe nanocrystals is that 1 mmol of CuCl reacts with 2 mmol of HDA in solution to make a Cu−HDA complex, but in the case of Ga^{3+} and In^{3+}, each millimole of the ions can form coordinate bonds with 3 or more mmol of HDA, and hence the complexes are more stable as compared to Cu−HDA complexes.[56] This leads to a higher reactivity of the Cu complexes in the solution, and hence Cu will first react with Se. According to the hard−soft acid−base model, elemental ions can be classified as acids and bases according to their capability to donate or accept electrons. These acids and bases again can be classified as hard and soft according to their polarizability, oxidation states, and electronegativity.[57] Therefore, Cu^+ is a soft acid and Se^{2-} is a soft base, and soft acids react faster and form stronger bonds with soft bases than hard acids with soft bases. Because Ga^{3+} is a harder acid as compared to In^{3+} because In^{3+} is more electronegative than Ga^{3+}, an In^{3+} precursor would bond easily to Se^{2-} to form amorphous In_2Se_3. Therefore, CuSe and In_2Se_3 are more likely to form at the initial stage of the reaction but not Ga_2Se_3. Ga−HDA complexes are available to react with CuSe in the solution to form $CuGaSe_2$. This was supported by the presence of small $CuGaSe_2$ nanocrystals at this point in the reaction. From our observation, $CuGaSe_2$ is very likely to evolve from CuSe particles reacting with the Ga^{3+} complex.

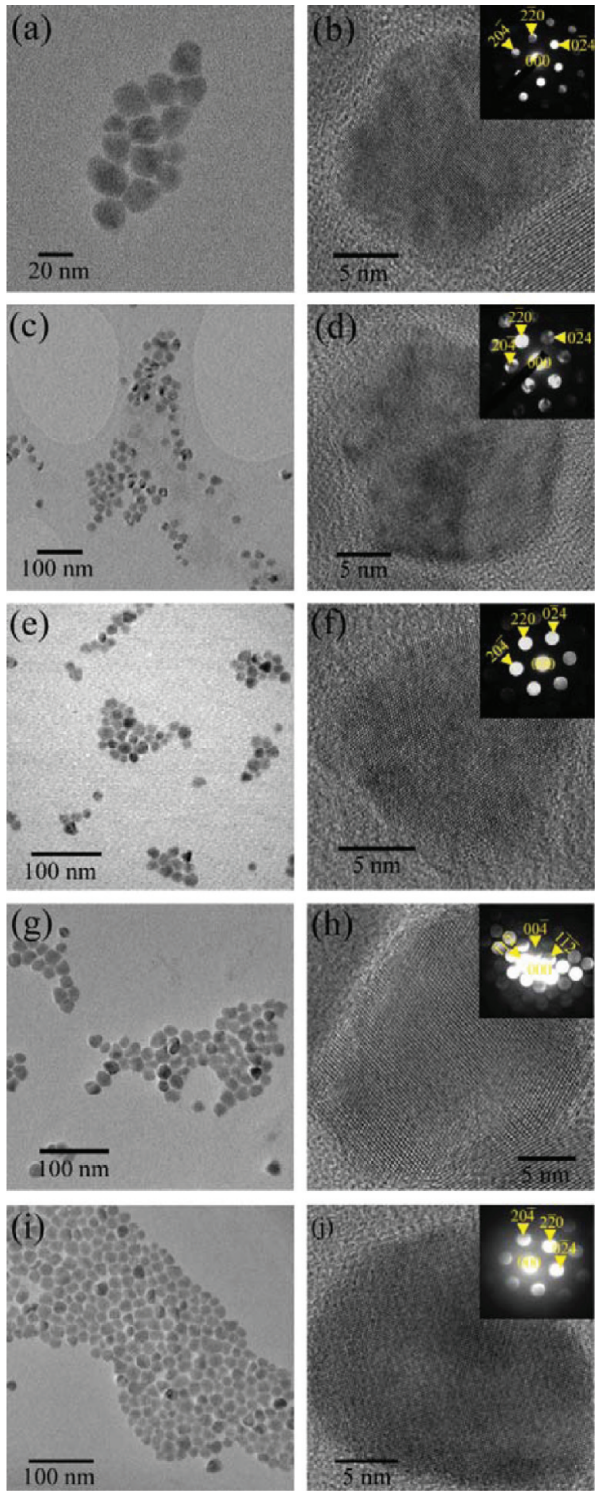

Figure 3. TEM images showing the different growth stages of $CuIn_xGa_{1-x}Se_2$ nanocrystals (a) 10 min at 130 °C, (c) 20 min at 160 °C, (e) 40 min at 200 °C, (g) 60 min at 230 °C, and (i) 120 min at 230 °C. (b), (d), (f), (h), and (j) are the corresponding HRTEM images and CBED patterns from the nanocrystals.

In the second stage as the temperature increased, Se nanorods dissolved, and In_2Se_3 dissociated. $CuIn_xGa_{1-x}Se_2$ was formed at the expense of CuSe. CuSe particles dissolved to provide the precursors for $CuIn_xGa_{1-x}Se_2$. As observed in

dx.doi.org/10.1021/jp300187r | J. Phys. Chem. C 2012, 116, 8202−8209

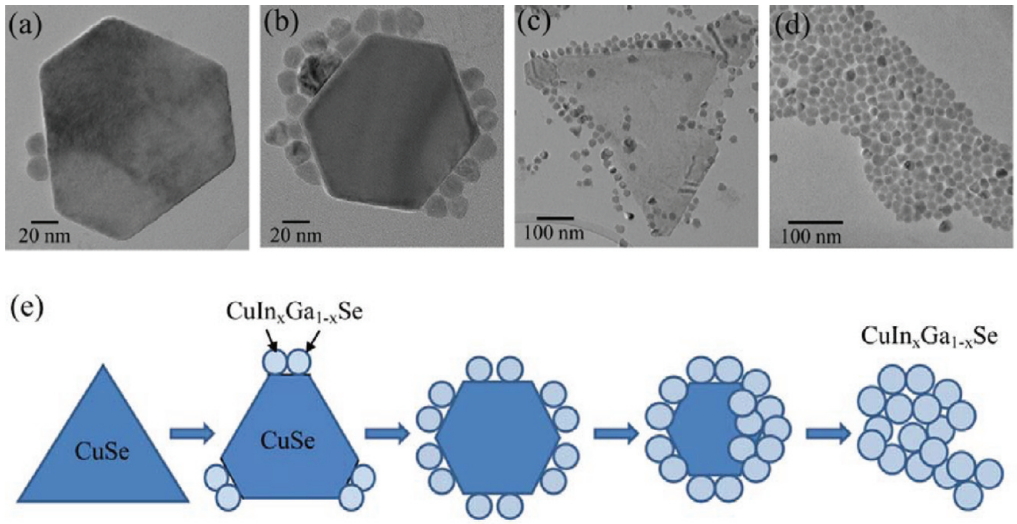

Figure 4. TEM images showing dissolution of CuSe nanoparticles and growth of $CuIn_xGa_{1-x}Se_2$ inside these particles at (a) 130 °C, (b) 160 °C, (c) 200 °C, and (d) 230 °C. (e) Proposed growth scheme for $CuIn_{0.5}Ga_{0.5}Se_2$ nanoparticles.

TEM images and the proposed schematic growth mechanism (Figure 4), large CuSe particles continuously dissolve as the reaction progressed to 200 °C. Stage 3 involved full dissolution of CuSe followed by the formation of two different CIGSe phases (Figure 4 and Table S1). This is a strong indication that CIGSe phases are more stable at higher temperature than CuSe. Another 60 min at 230 °C resulted in the equilibrium single phase of $CuIn_{0.5}Ga_{0.5}Se_2$ nanocrystals, and no obvious change in the shape of the particles was observed. Recently, Kar et al. showed that the formation of $CuInSe_2$ nanocrystals in oleylamine involved by the formation of CuSe and InSe nanocrystals as the primary intermediates.[45] Besides, the phase transformation of biphasic $Cu_2S-CuInS_2$ to monophasic $CuInS_2$ nanocrystals turned out to be an essential intermediate step.[58,59] Figure 5 shows the evolution of the crystal structure

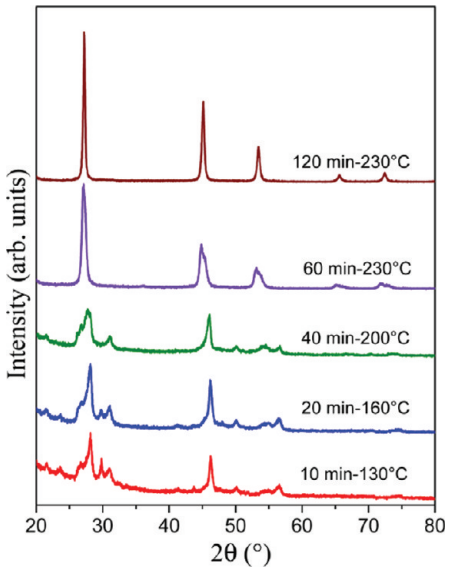

Figure 5. X-ray diffraction patterns showing the evolution of the crystal structure of $CuIn_xGa_{1-x}Se_2$.

to single-phase tetragonal $CuIn_{0.5}Ga_{0.5}Se_2$ as the temperature is changed.

Other than exploring the phase evolution of CIGSe, it is crucial to be able to determine the phase purity and stoichiometry to better tailor the optical properties of $CuIn_xGa_{1-x}Se_2$ nanocrystals. As it is not possible to deduce the site occupancy from XRD patterns of the nanocrystals, Vegard's law was used instead to predict the In/Ga stoichiometry. This is an empirical rule to determine the unit cell parameters of a solid-solution series in an alloy.[60] The unit cells for $CuIn_xGa_{1-x}Se_2$ are a = 5.614 ± 0.001 Å, c = 11.022 ± 0.001 Å, volume = 347.38 Å^3 when x = 0,[49] and a = 5.8011 ± 0.0001 Å, c = 11.6562 ± 0.0002 Å, volume = 392.26 Å^3 when x = 1.[48] A linear increase of the unit cell volume with x was expected as more In replaces Ga, and this trend was supported by the reported unit cell parameters of $CuIn_{0.52}Ga_{0.48}Se_2$.[50] The unit cell volume of intermediate compositions of $CuIn_xGa_{1-x}Se_2$ was found by interpolation, and the occupancy was determined. The a and c parameters were also determined to be quite close to the interpolated trend (Figure 6), except for $CuIn_xGa_{1-x}Se_2$ (x = 0.39) where the crystallite size was too small (~4 nm) leading to large estimated standard deviations in the unit cell parameters. At 230 °C (60 min), the products were 45 wt % $CuIn_{0.36}Ga_{0.64}Se_2$ and 55 wt % $CuIn_{0.64}Ga_{0.36}Se_2$ (Table S2), which is equivalent to the starting stoichiometric proportion of the reactants Cu:In:Ga:Se = 1:0.5:0.5:2. The crystallite size was obtained from a Rietveld refinement and was supported by TEM measurements (Figure 3g and h). The final monophasic $CuIn_xGa_{1-x}Se_2$ (x = 0.49) crystals had the $I\bar{4}2d$ space group (a = 5.6942 Å, c = 11.3876 Å, volume = 369.23 ± 0. 01 Å^3) and are in close agreement with reported $CuIn_{0.52}Ga_{0.48}Se_2$.[48]

To clearly differentiate between a solid solution of $CuIn_{0.5}Ga_{0.5}Se_2$ and immiscible 50 at. % $CuInSe_2$ and 50 at. % $CuGaSe_2$, XRD patterns of $CuInSe_2$, $CuGaSe_2$, and $CuIn_{0.5}Ga_{0.5}Se_2$ were calculated (Figure 7). At 2θ = 27.1° specifically, a solid solution of $CuIn_{0.5}Ga_{0.5}Se_2$ has a single (hkl) peak, while when two immiscible phases are present, the peak is split or a peak shoulder is observed. A split peak was observed after 60 min at 230 °C but disappears after 120 min. This can also be seen in some of the earlier publications[35,39] that reported on the single phase of $CuIn_xGa_{1-x}Se_2$. We believe that this split peak is characteristic of a biphasic $CuIn_xGa_{1-x}Se_2$

dx.doi.org/10.1021/jp300187r | J. Phys. Chem. C 2012, 116, 8202−8209

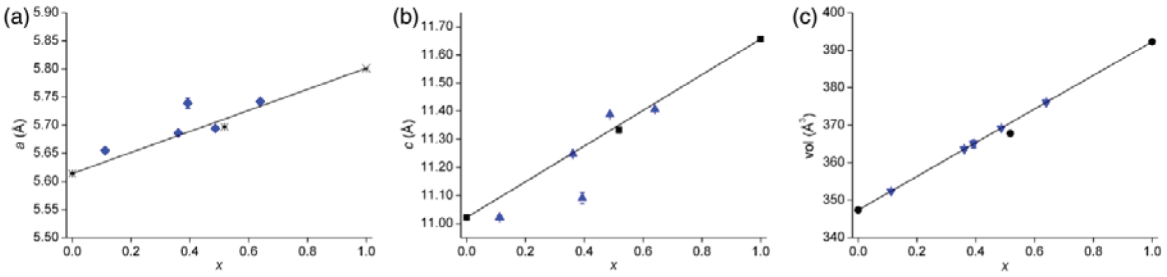

Figure 6. The effect of x in the different $CuIn_xGa_{1-x}Se_2$ compositions on the (a) unit cell parameter, a, (b) unit cell parameter, c, and (c) cell volume (the solid line represents Vegard's law). Black, reported data; blue, current study.

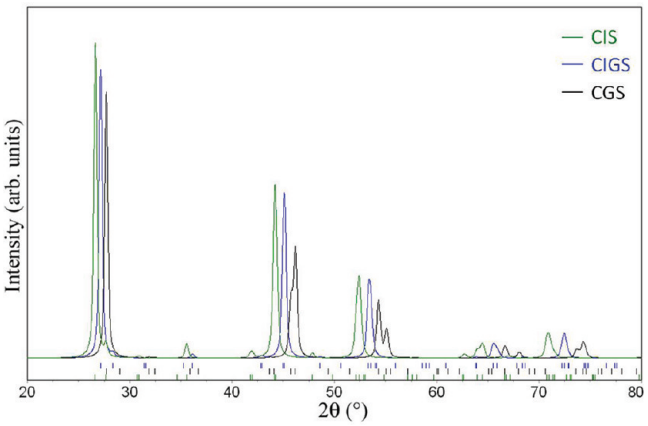

Figure 7. Calculated XRD patterns of $CuInSe_2$, $CuGaSe_2$, and $CuIn_{0.5}Ga_{0.5}Se_2$.

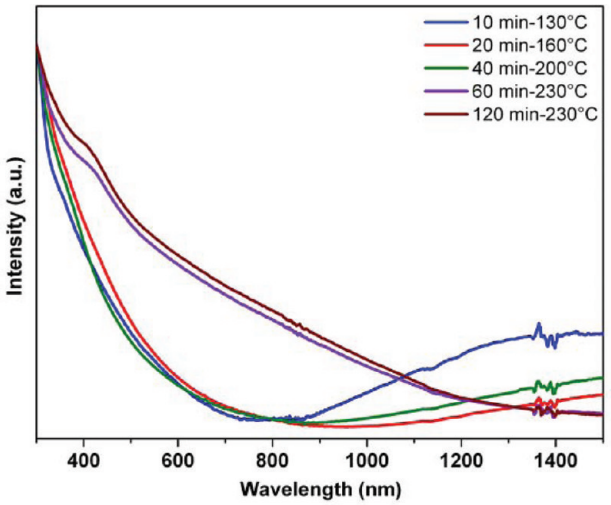

Figure 9. Room-temperature UV–vis absorption spectra of the samples at different stages of the reaction.

nanocrystal, and the two-phase model was able to account for the peaks very well (Figure 8).

3.3. Optical Characteristics of Cu–In–Ga–Se Systems. Another confirmation of the phase evolution can be obtained from the changes in the optical properties during the formation of the single band gap $CuIn_{0.5}Ga_{0.5}Se_2$ system.[61] Figure 9 shows the evolution of UV–vis absorption spectra of the aliquots taken at different times during the reaction. One can clearly see that the absorption edge of the five samples shifts to the right as the reaction temperature increases to 230 °C. All of the samples have strong absorption in the visible range extending to the infrared wavelengths.

There can be a number of reasons for the change in optical absorption properties. The optical absorption properties of nanoparticles are dependent on the size of the nanoparticles especially near the quantum confinement conditions and depend on the stoichiometry of the phases. In our study, the change in optical properties can be attributed to the presence of

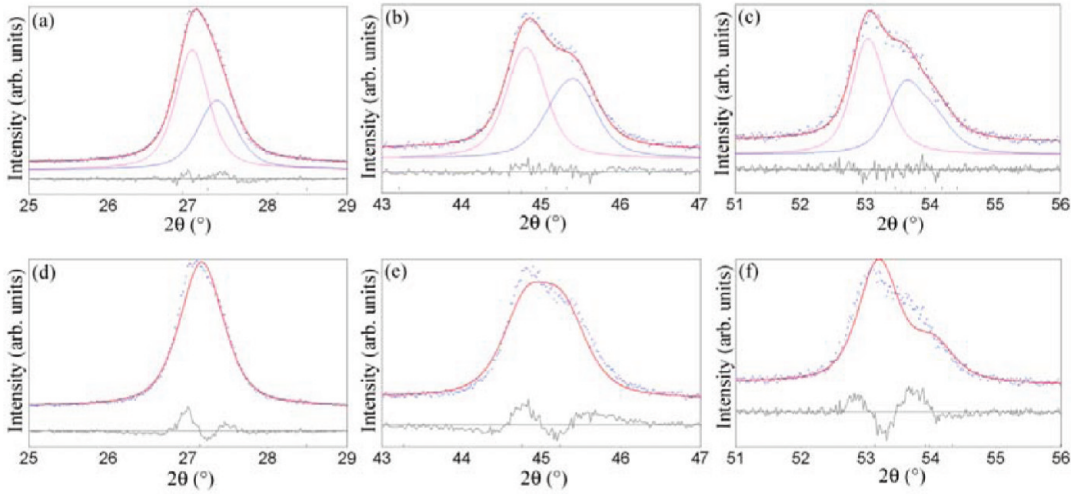

Figure 8. Rietveld refinement of $CuIn_xGa_{1-x}Se_2$ after 60 min at 230 °C near 2θ = 27.1°, 45.1°, and 53.4° using (a), (b), and (c) the two-phase model and (d), (e), and (f) the one-phase model.

dx.doi.org/10.1021/jp300187r | J. Phys. Chem. C 2012, 116, 8202–8209

different phases during the growth of $CuIn_{0.5}Ga_{0.5}Se_2$ nanocrystals as the particle sizes are beyond the quantum confinement regime, and hence the changes in absorption edges cannot be attributed to sizes. The red-shifted band edge of the particles as the reaction proceeds indicates the phase changes to $CuIn_{0.5}Ga_{0.5}Se_2$ (Figure 9).

On the basis of the stoichiometry of $CuIn_{1-x}Ga_xSe_2$ nanocrystals, it is possible to calculate their optical band gap. The fundamental transitions in the energy band gap for the different compositions of $CuIn_{1-x}Ga_xSe_2$ are fitted to an equation:[62]

$$E_g = 1.010 + 0.626x - 0.167x(1 - x) \quad (2)$$

The energy band gap (E_g) for $CuIn_{0.49}Ga_{0.51}Se_2$ extracted from UV–vis spectroscopy is close to the calculated values (eq 2) (Table 1). For the biphasic sample (230 °C, 60 min), the

Table 1. Comparison of the Calculated and Extracted Energy Band Gap from UV–Vis Spectroscopy of the Samples at 230 °C

temperature/time		calculated energy band gap from eq 2 (eV)		energy band gap extracted from UV–vis spectroscopy (eV)
230 °C/ 60 min	$CuIn_{0.64}Ga_{0.36}Se_2$ (45 wt %)	1.19	ave 1.29	1.2
	$CuIn_{0.36}Ga_{0.64}Se_2$ (55 wt %)	1.37		
230 °C/ 120 min	$CuIn_{0.49}Ga_{0.51}Se_2$	1.28		1.2

energy band gap is split into two values depending on x, and the average energy band gap considering the weight proportion of each phase is close to $CuIn_{0.49}Ga_{0.51}Se_2$. For shorter reaction times and lower temperatures, the energy band gap is shifted toward higher energy, due to the contribution from CuSe (E_g = 2 eV)[63] (see Supporting Information Figure S4). From the UV–vis measurements, a single energy band gap does not correlate to the single phase and can be observed for both mono and biphasic $CuIn_xGa_{1-x}Se_2$. Hence, a careful crystallochemical study may overcome the limits of optical absorption measurements, and this might help tailor the desired properties for solar cell applications.

4. CONCLUSIONS

A systematic study of the formation process of $CuIn_{0.5}Ga_{0.5}Se_2$ nanocrystals prepared using the hot coordination method has been described. This understanding will provide a means to control the synthesis of a pure, single-phase quaternary compound. The reaction started with the formation of crystalline CuSe, Se, $CuGaSe_2$, and amorphous In_2Se_3. From this work, we can see that $CuIn_{0.5}Ga_{0.5}Se_2$ evolved from the CuSe phase. A possible growth mechanism to explain the formation of $CuIn_{0.5}Ga_{0.5}Se_2$ was proposed. The resulting $CuIn_{0.5}Ga_{0.5}Se_2$ nanoparticles are highly uniform in composition and phase. The phase purity was confirmed by Rietveld refinement and the uniformity in composition deduced from Vegard's law because occupancy refinement cannot give a satisfactory measurement of the In and Ga stoichiometry. The high phase purity determined from the X-ray data implies that single band gap $CuIn_{0.5}Ga_{0.5}Se_2$ had been obtained, and this control offers the possibility of tuning the band gap of this material for application in photovoltaic cells.

■ ASSOCIATED CONTENT

Supporting Information

(1) TEM images and EDX spectra of amorphous In_2Se_3 and Se nanorods, (2) HRTEM and corresponding diffraction patterns of CuSe nanocrystals at different temperatures, (3) an extrapolation of the UV–vis spectra of the samples at different stages of the reaction, (4) refined crystallite size and weight percentage of each constituent shown at each step of the reaction, and (5) refined unit cell parameters of $CuIn_xGa_{1-x}Se_2$ with temperature–time variation. This material is available free of charge via the Internet at http://pubs.acs.org.

■ AUTHOR INFORMATION

Corresponding Author

*Fax: +65 6790 9081. E-mail: ymlam@ntu.edu.sg.

Notes

The authors declare no competing financial interest.

■ ACKNOWLEDGMENTS

This work was supported by the Agency for Science, Technology and Research (A*STAR-Singapore) and the Energy Research Institute at Nanyang Technological University.

■ REFERENCES

(1) Schmid, G. *Nanoparticles: From Theory to Applications*; Wiley-VCH: Weinheim, Germany, 2004.
(2) Fukumori, H.; Ichikawa, H. *Adv. Powder Technol.* **2006**, *17*, 1–28.
(3) Murray, C. B.; Norris, D. J.; Bawendi, M. G. *J. Am. Chem. Soc.* **1993**, *115*, 8706–8715.
(4) Alivisatos, A. P. *Science* **1996**, *271*, 933–937.
(5) Henglein, A. *Chem. Rev.* **1989**, *89*, 1861–1873.
(6) Hines, M. A.; Guyot-Sionnest, P. *J. Phys. Chem. B* **1998**, *102*, 3655–3657.
(7) Trinidade, T.; O'Brien, P.; Pickett, N. L. *Chem. Mater.* **2001**, *13*, 3843–3858.
(8) Qu, L.; Peng, Z. A.; Peng, X. *Nano Lett.* **2001**, *1*, 333–337.
(9) English, D. S.; Pell, L. E.; Yu, Z.; Barbara, P. F.; Korgel, B. A. *Nano Lett.* **2002**, *2*, 681–685.
(10) Gerion, D.; Zaitseva, N.; Saw, C.; Casula, M. F.; Fakra, S.; Van Buuren, T.; Galli, G. *Nano Lett.* **2004**, *4*, 597–602.
(11) Battaglia, D.; Peng, X. *Nano Lett.* **2002**, *2*, 1027–1030.
(12) Talapin, D. V.; Rogach, A. L.; Mekis, I.; Haubold, S.; Kornowski, A.; Haase, M.; Weller, H. *Colloids Surf. A* **2002**, *202*, 145–154.
(13) Micic, O. I.; Ahrenkiel, S. P.; Bertram, D.; Nozik, A. J. *Appl. Phys. Lett.* **1999**, *75*, 478–480.
(14) Huynh, W. U.; Dittmer, J. J.; Alivisatos, A. P. *Science* **2002**, *295*, 2425–2427.
(15) Arici, E.; Meissner, D.; Schaffler, F.; Sariciftci, N. S. *Int. J. Photoenergy* **2003**, *5*, 199–208.
(16) Gur, I.; Fromer, N. A.; Geier, M. L.; Alivisatos, A. P. *Science* **2005**, *310*, 462–465.
(17) Kumar, S.; Scholes, G. D. *Microchim. Acta* **2008**, *160*, 315–325.
(18) Duan, X.; Huang, Y.; Agarwal, R.; Lieber, C. M. *Nature* **2003**, *421*, 241–245.
(19) Pan, Z. W.; Dai, Z. R.; Wang, Z. L. *Science* **2001**, *291*, 1947–1949.
(20) Rogach, A. L.; et al. *Angew. Chem., Int. Ed.* **2008**, *47*, 6538–6549.
(21) Zhong, H.; Wang, Z.; Bovero, E.; Lu, Z.; van Veggel, F. C. J. M.; Scholes, G. D. *J. Phys. Chem. C* **2011**, *115*, 12396–12402.
(22) Alivisatos, P. *Nat. Biotechnol.* **2004**, *22*, 47–52.
(23) Wei, S.-H.; Zhang, S. B.; Zunger, A. *Appl. Phys. Lett.* **1998**, *72*, 3199–3201.
(24) Guezmir, N.; Ouerfelli, J.; Belgacem, S. *Mater. Chem. Phys.* **2006**, *96*, 116–123.

(25) Czekelius, C.; Hilgendorff, M.; Spanhel, L.; Bedja, I.; Lerch, M.; Muller, G.; Bloeck, U.; Su, D. S.; Giersig, M. *Adv. Mater.* **1999**, *11*, 643−646.
(26) Arici, E.; Sariciftci, N. S.; Meissner, D. *Adv. Funct. Mater.* **2003**, *13*, 165−171.
(27) Guo, Q.; Kim, S. J.; Kar, M.; Shafarman, W. N.; Birkmire, R. W.; Stach, E. A.; Agrawal, R.; Hillhouse, H. W. *Nano Lett.* **2008**, *8*, 2982−2987.
(28) Guo, Q.; Ford, G. M.; Hillhouse, H. W.; Agrawal, R. *Nano Lett.* **2009**, *9*, 3060−3065.
(29) Joo, J.; Na, H. B.; Yu, T.; Yu, J. H.; Kim, Y. W.; Wu, F.; Zhang, J. Z.; Hyeon, T. *J. Am. Chem. Soc.* **2003**, *125*, 11100−11105.
(30) Gautam, U. K.; Seshadri, R. *Mater. Res. Bull.* **2004**, *39*, 669−676.
(31) Hyeon, T. *Chem. Commun.* **2003**, *8*, 927−934.
(32) Wang, X.; Pan, D.; Weng, D.; Low, C.-Y.; Rice, L.; Han, J.; Lu, Y. *J. Phys. Chem. C* **2010**, *114*, 17293−17297.
(33) Panthani, M. G.; Akhavan, V.; Goodfellow, B.; Schmidtke, J. P.; Dunn, L.; Dodabalapur, A.; Barbara, P. F.; Korgel, B. A. *J. Am. Chem. Soc.* **2008**, *130*, 16770−16777.
(34) Tang, J.; Hinds, S.; Kelley, S. O.; Sargent, E. H. *Chem. Mater.* **2008**, *20*, 6906−6910.
(35) Wang, Y.-H. A.; Pan, C.; Bao, N.; Gupta, A. *Solid State Sci.* **2009**, *11*, 1961−1964.
(36) Zhong, H.; Li, Y.; Ye, M.; Zhu, Z.; Zhou, Y.; Yang, C.; Li, Y. *Nanotechnology* **2007**, *18*, 025602.
(37) Ghezelbash, A.; Korgel, B. A. *Langmuir* **2005**, *21*, 9451−9456.
(38) Sun, S.; Murray, C. B.; Weller, D.; Folks, L.; Moser, A. *Science* **2000**, *287*, 1989−1992.
(39) Al Juhaiman, L.; Scoles, L.; Kingston, D.; Patarachao, B.; Wang, D.; Bensebaa, F. *Green Chem.* **2010**, *12*, 1248−1252.
(40) Gu, S. I.; Hong, S. H.; Shin, H. S.; Hong, Y. W.; Yeo, D. H.; Nahm, S. *J. Korean Phys. Soc.* **2010**, *57*, 1059−1061.
(41) Talapin, D. V.; Rogach, A. L.; Kornowski, A.; Haase, M.; Weller, H. *Nano Lett.* **2001**, *1*, 207−211.
(42) Qu, L.; Peng, X. *J. Am. Chem. Soc.* **2002**, *124*, 2049−2055.
(43) de Mello Donega, C.; Hickey, S. G.; Wuister, S. F.; Vanmaekelbergh, D.; Meijerink, A. *J. Phys. Chem. B* **2003**, *107*, 489−496.
(44) Norako, M. E.; Franzman, M. A.; Brutchey, R. L. *Chem. Mater.* **2009**, *21*, 4299−4304.
(45) Kar, M.; Agrawal, R.; Hillhouse, H. W. *J. Am. Chem. Soc.* **2011**, *133*, 17239−17247.
(46) Stolen, S.; Fjellvag, H.; Gronvold, F.; Sipowska, J. T.; Westrum, E. F. *J. Chem. Thermodyn.* **1996**, *28*, 753−766.
(47) McCann, D. R.; Cartz, L. *J. Appl. Phys.* **1972**, *43*, 4473−4477.
(48) Schorr, S.; Geandier, G. *Cryst. Res. Technol.* **2006**, *41*, 450−457.
(49) Mandel, L.; Tomlinson, R. D.; Hampshire, M. J. *J. Appl. Crystallogr.* **1977**, *10*, 130−131.
(50) Souilah, M.; Rocquefelte, X.; Lafond, A.; Guillot-Deudon, C.; Morniroli, J. P.; Kessler, J. *Thin Solid Films* **2009**, *517*, 2145−2148.
(51) Hill, R. J.; Howard, C. J. *J. Appl. Crystallogr.* **1987**, *20*, 467−474.
(52) Pan, D.; Wang, X.; Zhou, Z. H.; Chen, W.; Xu, C.; Lu, Y. *Chem. Mater.* **2009**, *21*, 2489−2493.
(53) Pan, D.; An, L.; Sun, Z.; Hou, W.; Yang, Y.; Yang, Z.; Lu, Y. *J. Am. Chem. Soc.* **2008**, *130*, 5620−5621.
(54) Rietveld, H. M. *Acta Crystallogr.* **1967**, *22*, 151−152.
(55) Stokes, A. R.; Wilson, A. J. C. *Proc. Cambridge Philos. Soc.* **1942**, *38*, 313.
(56) Burkin, A. R. *J. Chem. Soc.* **1950**, 127−132.
(57) Pearson, R. G. *J. Am. Chem. Soc.* **1963**, *85*, 3533−3539.
(58) Kruszynska, M.; Borchert, H.; Parisi, J.; Kolny-Olesiak, J. *J. Am. Chem. Soc.* **2010**, *132*, 15976−15986.
(59) Connor, S. T.; Hsu, C.-M.; Weil, B. D.; Aloni, S.; Cui, Y. *J. Am. Chem. Soc.* **2009**, *131*, 4962−4966.
(60) Vegard, L.; Schjelderup, H. *Z. Phys.* **1917**, *18*, 93.
(61) Dai, P.; Shen, X.; Lin, Z.; Feng, Z.; Xu, H.; Zhan, J. *Chem. Commun.* **2010**, *46*, 5749−5751.
(62) Alonso, M. I.; Garriga, M.; Durante Rincon, C. A.; Hernandez, E.; Leon, M. *Appl. Phys. A: Mater. Sci. Process.* **2002**, *74*, 659−664.
(63) Pejova, B.; Grozdanov, I. *J. Solid State Chem.* **2001**, *158*, 49−54.